2014

Influence of the Sea Surface Microlayer on Ozone Deposition Velocity

Kathryn Moore
Colby College

Influence of the Sea Surface Microlayer on Ozone Deposition Velocity

Kathryn A. Moore

A Thesis Presented to the Department of Chemistry,
Colby College, Waterville, ME
In Partial Fulfillment of the Requirements for Graduation
With Honors in Chemistry

Submitted May 2014

Kathryn was born in Alexandria, Virginia, to Susan Hess and Daniel Moore, and spent her childhood moving between US State Department posts in New Delhi, India, Kuala Lumpur, Malaysia, Taipei, Taiwan, and Washington, D.C. She began high school at Taipei American School in Taipei and graduated from Thomas Jefferson High School for Science and Technology in Virginia in 2010. She then attended Colby College, where she majored in chemistry and minored in physics, graduating with a Bachelor of Arts in 2014. While at Colby, she was a member of the Equestrian Club and captain of the Ultimate Frisbee team. During her sophomore year at Colby, Kathryn worked in the Thamattoor lab, developing a new synthetic route to alkylidenecarbenes via photolysis of cyclopropanated phenanthrene derivatives. During her junior year, she participated in a semester program at Bigelow Laboratory for Ocean Sciences; the relationship continued into her senior year and culminated in this honors thesis.

Acknowledgements

I would like to thank Drs. Steve Archer and Paty Matrai for the opportunity to conduct research in their lab over the past two years. Without their support, guidance, and assistance, this project would not have been possible. I would also like to thank Professor Whitney King for his advice and support throughout my time at Colby and his insightful comments during all stages of this work. I also owe a great deal to Professor Nick Boekelheide for his assistance with Matlab, discussions on theory and modeling, and encouragement throughout this year. Finally, I would like to thank Nick Record at Bigelow for his advice on coding in Matlab, and Randy Downer at Colby for helping me through all the technical difficulties encountered during this year.

Table of Contents

List of Tables and Figures

Abstract

The biogeochemical cycles of both iodine and ozone are strongly linked to human health and global climate and are tightly coupled through chemical processes occurring in the surface ocean and troposphere. The concentration and distribution of these compounds have the potential to drive the oxidizing capacity and suite of chemical reactions occurring in the marine boundary layer. However, modeling coupled ocean-atmosphere systems involving them is challenging because of a limited understanding of the magnitude and dominant mechanisms controlling the fluxes of both species, in addition to temporally and spatially heterogeneous distributions of ozone and iodine in the sea surface and lower troposphere. Recent modeling studies have suggested a 30% contribution of halogen chemistry to overall oceanic ozone deposition, which is equivalent to an average annual cooling of 0.1 W m^{-2}, or 30% of the warming effect of tropospheric ozone. This has the potential to appreciably alter the radiative balance of the atmosphere, with broad implications for global climate. A laboratory-based experimental approach was used to explore the role of organic microlayers at the air-water interface in mediating the sea-surface reaction between ozone and iodide. Films of stearic acid, an insoluble fatty acid, were shown to significantly reduce the rate of ozone deposition to both phosphate-buffered solutions and natural seawater. Taken in conjunction with the proportionality between iodide concentration and ozone deposition velocity, regional variability in the concentrations of iodide and insoluble organics have the potential to influence global fluxes of ozone and volatile iodinate compounds, and thus impact tropospheric chemistry and radiative forcing.

1 Introduction

1.1 Overview

Although more commonly viewed as a ground-level pollutant or the component of the stratosphere responsible for limiting the amount of harmful UVB and UVC radiation that reaches Earth's surface, ozone is also present throughout the troposphere, where it is a potent greenhouse gas and one of the largest contributors to atmospheric radiative forcing (Fig. 1).[1,2]

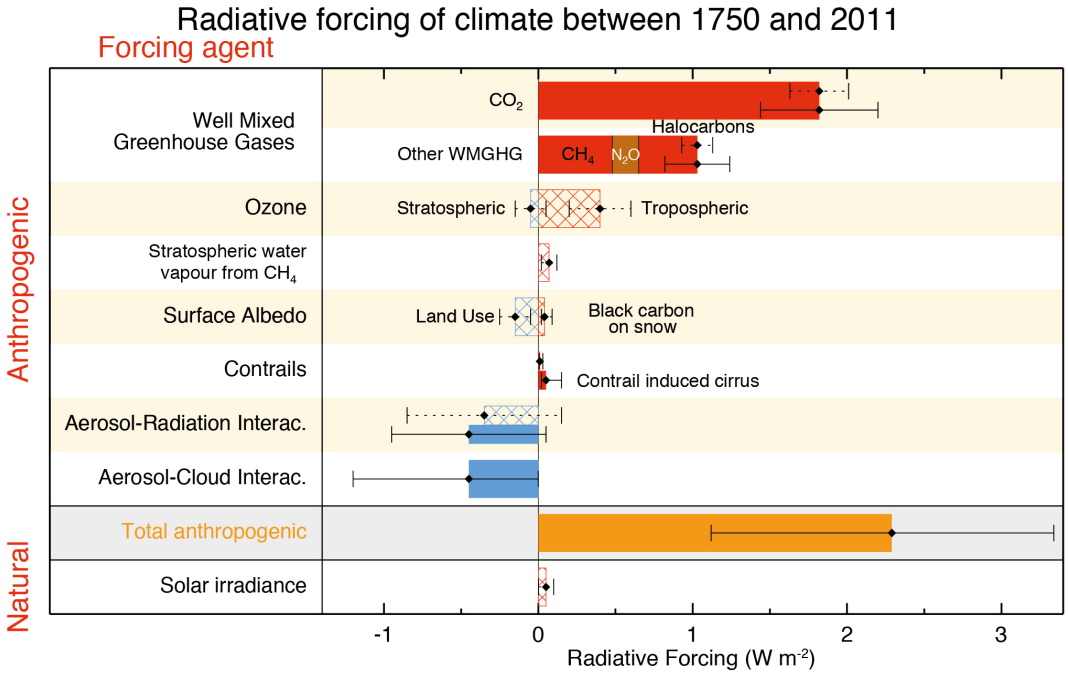

Figure 1. Bar chart for RF (radiative forcing, hatched) and ERF (effective radiative forcing, solid) for the period 1750–2011. Uncertainties (5 to 95% confidence range) are given for RF (dotted lines) and ERF (solid lines).[1]

Background concentrations of ozone in the Northern Hemisphere have more than doubled since the late 19th century, with similar increases globally; as a consequence, the radiative forcing from tropospheric ozone has also increased during this period (Fig. 2).[1,2] Although a deceleration in the time evolution of radiative forcing due to tropospheric ozone is observed beginning around 1990 as a result of decreases in anthropogenic emissions of precursors, the radiative forcing

associated with tropospheric ozone is predicted to continue to increase in the coming decades; hence, its global distribution is an important factor in climate models.[1] Ozone plays a large role in tropospheric chemistry, particularly photochemical reactions and those involving halogens, and its concentration is strongly influenced by those of other atmospheric chemical species.[1-3] One area of particular interest is the coupling of the ozone and iodine biogeochemical cycles through processes occurring in the surface ocean and troposphere.

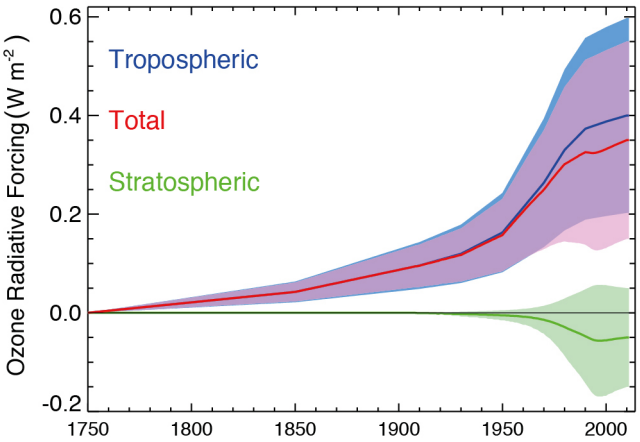

Figure 2. Time evolution of the radiative forcing from tropospheric and stratospheric ozone from 1750 to 2010. Tropospheric ozone data are from Stevenson et al. (2013) scaled to give 0.40 W m^{-2} at 2010. The stratospheric ozone RF follow the functional shape of the Effective Equivalent Stratospheric Chlorine assuming a 3-year age of air (Daniel et al., 2010) scaled to give –0.05 W m^{-2} at 2010.[1]

Ozone, iodine, and related species undergo complex redox and photochemical reactions in the lower troposphere and ocean surface, and the concentration, distribution and speciation of these compounds have the potential to significantly influence the overall suite of chemical reactions occurring in, as well as the oxidizing capacity of, the lower marine boundary layer (MBL).[2,4] However, modeling coupled ocean-atmosphere systems involving these compounds is challenging because the magnitude and dominant mechanisms influencing the fluxes of both species are not well understood, in addition to being spatially and temporally heterogeneous.[5-6]

Recent modeling studies have suggested a 30% contribution of halogen chemistry to overall oceanic ozone deposition, which is equivalent to an average annual cooling of 0.1 W m^{-2}, or 30% of the warming effect of tropospheric ozone.[5] This has the potential to appreciably alter the radiative balance of the atmosphere, with broad implications for global climate. One of the major reactions responsible for this deposition is the heterogeneous sea surface reaction between ozone and iodide, which leads to the destruction of ozone and the production of I_2 (Eq. 1-2).

$$H^+ + I^- + O_3(g) \rightarrow HOI(aq) + O_2(g) \quad (1)$$

$$H^+ + HOI(aq) + I^-(aq) \leftrightarrow I_2(aq) + H_2O \quad (2)$$

Since this reaction occurs at the sea surface, the presence of a sea surface microlayer, or hydrated gelatinous layer 10s-100s of μm thick at the air-water interface, is expected to influence the rate and magnitude of this reaction by altering reactant diffusivity and concentration, and perhaps reaction mechanism(s).[7-10] The sea surface microlayer, being primarily composed of hydrophobic species and surfactants, as well as being located at the top of the water column, represents a physico-chemical environment that differs significantly from the subsurface water.[8-10] Although shown to be significant in photochemical or photosensitized surface reactions,[7,11] the role of a sea surface microlayer in the reaction between ozone and iodide is not well understood. If important in controlling the rate or magnitude of the reaction between ozone and iodine, the presence and composition of such microlayers may have the potential to change tropospheric ozone budgets, and thus alter the predictions of climate models.

1.2 Biogeochemical Cycles of Iodine and Ozone

1.2.1 Biogeochemical Cycle of Iodine

The biogeochemical cycling of iodine is linked to environmental and human health considerations,[4] including contributions to atmospheric ozone destruction and deposition to the sea surface,[12-14] tropospheric oxidizing capacity,[12] aerosol particle formation,[15] and availability of iodine to terrestrial biology[15]. Iodine enters the ocean through riverine and groundwater inputs, and exists in several redox states, including iodide (I^-), iodate (IO_3^-), hypoiodous acid (HOI), and molecular iodine (I_2), with an approximate total concentration of 450nM (Fig. 3).[16]

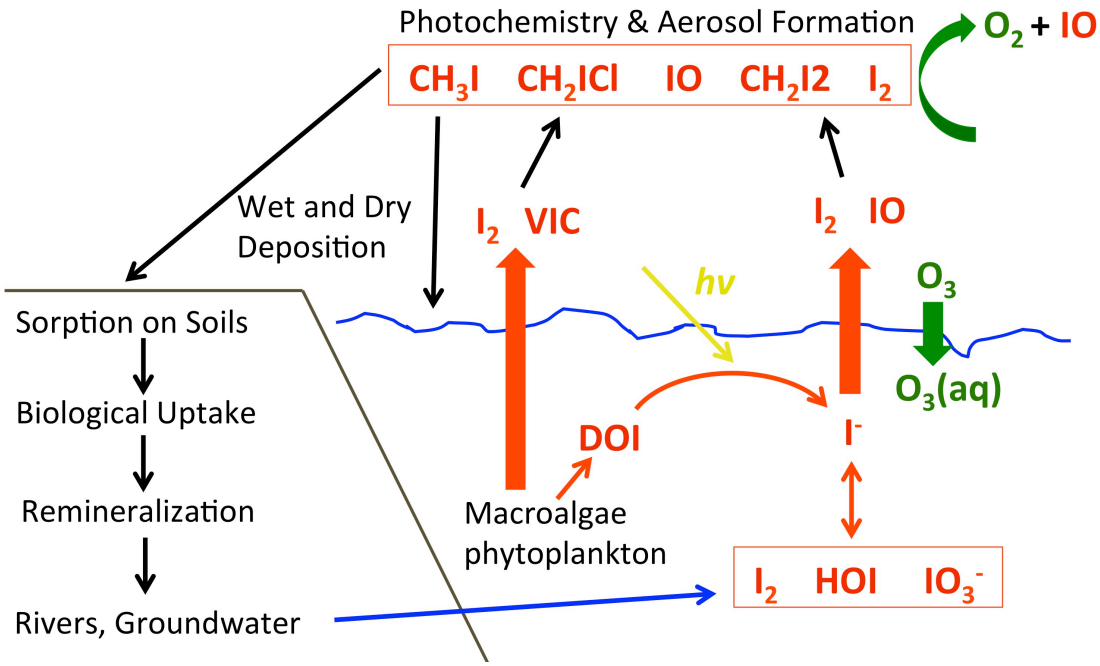

Figure 3. Simplified model of the biogeochemical cycle of iodine, with emphasis on the important chemical species in the upper ocean and lower troposphere.

Iodate is the dominant redox state of iodine in the marine upper water column, followed by iodide, although iodide is preferentially concentrated in the sea surface microlayer as a result of biologically mediated oxidation processes that occur near the ocean surface.[16-17] This is further enhanced by the release of dissolved organic iodine species (DOI) by macroalgae and

phytoplankton to the upper water column, which can subsequently be photochemically degraded to iodide.[17] In addition to iodide and iodate, molecular iodine can also be observed near the sea surface as a result of chemical and biological processes. In the presence of excess iodide, molecular iodine is expected to be in equilibrium with triiodide (Eq. 3), and the large, polarizable nature of both species leads to their concentration near the sea surface.[18]

$$I_2(aq) + I^-(aq) \leftrightarrow I_3^-(aq) \quad (3)$$

Oceanic sources of reactive iodine are major inputs to atmospheric and terrestrial pools, with CH_3I, CH_2ICl, CH_2I_2, and I_2 dominating the sea-to-atmosphere flux of volatile iodinated compounds (VICs).[15,19-21] Both biological and abiotic sources and sinks of VICs are implicated in controlling the flux of iodine across the sea-air boundary, particularly the release of VICs by macroalgae and photochemical reactions at the ocean surface, although determining the dominant mechanisms responsible for these fluxes has proved challenging.[15-16,22-24] In addition, substantial uncertainty still exists with regard to the magnitude of oceanic VIC emissions and how such emissions should be integrated into current atmospheric models.[25] Once in the atmosphere, reactive iodine compounds undergo a complex set of oxidative, photochemical, and other reactions, in addition to aerosol and particle formation, followed by deposition back to the ocean and terrestrial surface.

1.2.2 Biogeochemical Cycle of Ozone

Ozone is produced in both the stratosphere and troposphere, although through separate mechanisms, and has different implications for global climate and human health in each region of the atmosphere.[2-3] Stratospheric ozone, which comprises approximately 90% of the ozone in

the atmosphere and acts to prevent harmful UV radiation from reaching Earths' surface, is produced through the photolysis of molecular oxygen (Eq. 4-5).[3]

$$O_2 + h\nu_{\lambda<242nm} \rightarrow 2O(^3P) \quad (4)$$

$$O(^3P) + O_2 + M \rightarrow O_3 + M \quad (5)$$

The loss of stratospheric ozone occurs through reaction with atomic oxygen, photolysis, transfer into the troposphere, and catalytic destruction via reaction with trace gases such as chlorine, bromine, and nitrogen oxides.[3]

Ozone in the troposphere acts as a potent greenhouse gas, and is the third most important contributor to atmospheric radiative forcing.[2] Mid-level tropospheric ozone strongly influences the rate and magnitude of atmospheric photochemical reactions, while ground level ozone is considered a pollutant and has negative effects on human health and crop production.[2-3] In the troposphere, the NO/NO_2 cycle produces oxygen radicals through the photochemical dissociation of NO_2, which react with molecular oxygen to produce ozone (Fig. 4).[2-3] Rapid re-oxidation to NO_2 would tend to lead to a photostationary steady state concentration; however, coupling this process with the hydroxyl-peroxy (HO_x) radical cycle and the simultaneous oxidation of hydrocarbons or carbon monoxide allows for the net production of ozone.[3] The ozone thus produced participates in photochemical reactions and wet and dry deposition to ocean and terrestrial surfaces, in addition to other chemical reactions, notably involving halogens.[2-6,26-27] Tropospheric ozone is also a significant source of reactive intermediates through photolysis and subsequent reactions; the compounds thus generated play a role in a wide array of tropospheric chemical processes.

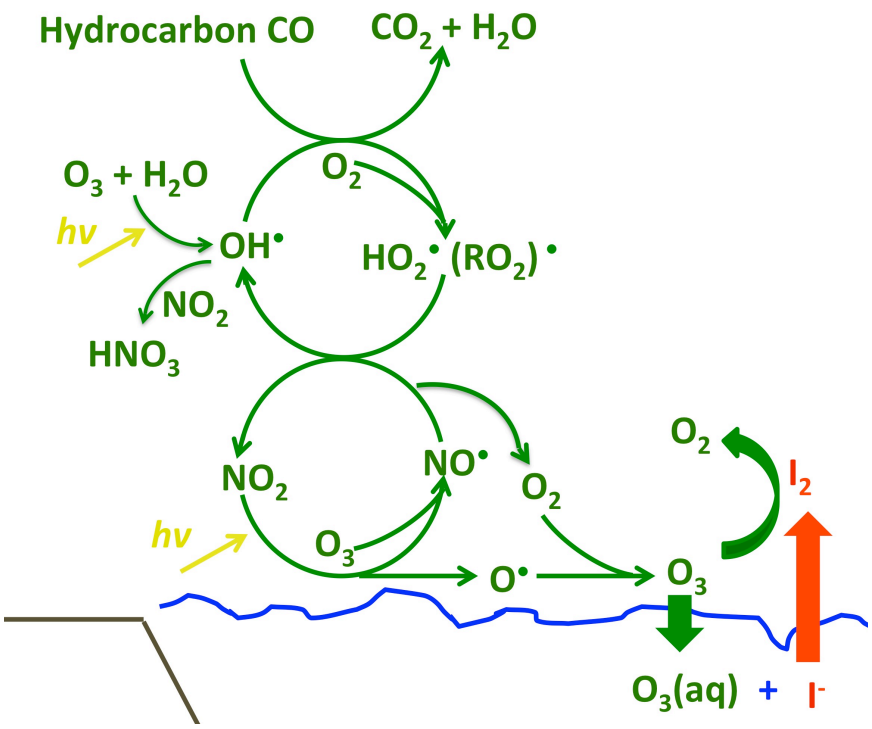

Figure 4. Model of ozone cycling in the troposphere. The lower loop is the NO/NO_2 cycle, which can be coupled to the hydroxyl-peroxy (HO_x) radical cycle and the oxidation of hydrocarbons or carbon monoxide to give net ozone production. The ozone thus produced reacts with species in the atmosphere or ocean surface, or undergoes dry or wet deposition.

1.2.3 Coupling of Ozone and Iodine Biogeochemical Cycles

Deposition of ozone to the ocean surface represents approximately one third of the 600-1000 Tg deposited annually[28], and is strongly dependent on halogen chemistry;[2-6,26-27] more specifically, reactions between VICs and O_3 are estimated to account for 20% of total ozone deposition to the sea surface.[14] Additionally, relative to global chemistry models that include photochemistry but exclude halogen chemistry, observed ozone loss rates in the tropical MBL were found to be 50% greater than in model simulations, with the majority of the additional loss (~75%) attributed to iodine.[12] Recent modeling studies have suggested a 30% contribution of halogen chemistry to overall oceanic ozone deposition, which is equivalent to an average annual cooling of 0.1 W m^{-2},

or 30% of the warming effect of tropospheric ozone.[5] This has the potential to appreciably alter the radiative balance of the atmosphere, with broad implications for global climate (Fig. 1).

Many of the atmospheric reactions between ozone and iodine occur as a result of the photodissociation of monohalogenated (CH_3I, C_2H_5I) and polyhalogenated (CH_2I_2, CH_2BrI, CH_2ClI) organics or molecular iodine (I_2) to form iodine radicals.[29] Iodine monoxide (IO) is the major product of these reactions (Fig. 3) and as such, high IO concentrations signal the destruction of ozone[29] (Eq. 6).

$$I^- + O_3 \rightarrow IO + O_2 \qquad (6)$$

Currently, known sources of reactive iodine cannot account for either the IO generated or ozone depleted in the tropical MBL.[30] Reactions occurring at the sea surface are proposed to generate the missing reactive iodide and to constrain the steady state tropospheric ozone concentration by enhancing chemical deposition.[31] However, this reaction is predicted to be significantly influenced in terms of rate and magnitude by the presence and composition of a sea surface microlayer, which may have an impact on tropospheric ozone budgets and chemical processes. This also provides a mechanism through which seasonal and locational variability in marine microbial ecology and associated organic compounds in the sea surface microlayer might factor into ozone and iodine fluxes across the air-water interface.

1.3 Sea Surface Microlayer

1.3.1 Overview

The presence of a sea surface microlayer, or a thin, distinct layer at the air-sea interface, was first proposed by John Sieburth in 1983.[32] This microlayer, or the top 10s to 100s of micrometers of the ocean, has since been shown to be physico-chemically distinct from subsurface water, and to contain unique microbial communities.[8-10] Consistent enrichment of biogenic and inorganic surface-active compounds, or surfactants, has been observed in the sea surface microlayer relative to the subsurface water at wind speeds between 5 and 10 m s^{-1}.[10] Significantly, its increased enrichment under oligotrophic conditions as well as its persistence under wind conditions exceeding the global average over the ocean[33], suggest that, at any given time, a microlayer may cover a significant portion of the ocean surface, potentially greater than 70%[30]. The principal components of the sea surface microlayer are polysaccharides released as photosynthetic exudates from phytoplankton and bacteria, which aggregate into biophysical gels and form a complex hydrated gelatinous film at the sea surface (Fig. 5).[9,34] In addition to polysaccharides, lipids, proteins, humic materials, trace metals, and other organic and inorganic compounds are also concentrated in the microlayer, which has been shown to play a role in air-sea gas and heat exchange[8], the production of organic-rich aerosols[35], and biogeochemical cycles[36]. Due to its position at the air-water interface, the composition of the sea surface microlayer is not static, but is constantly being altered by biological and physical mediation, particularly through wave action, bubble bursting, and aerosol production.

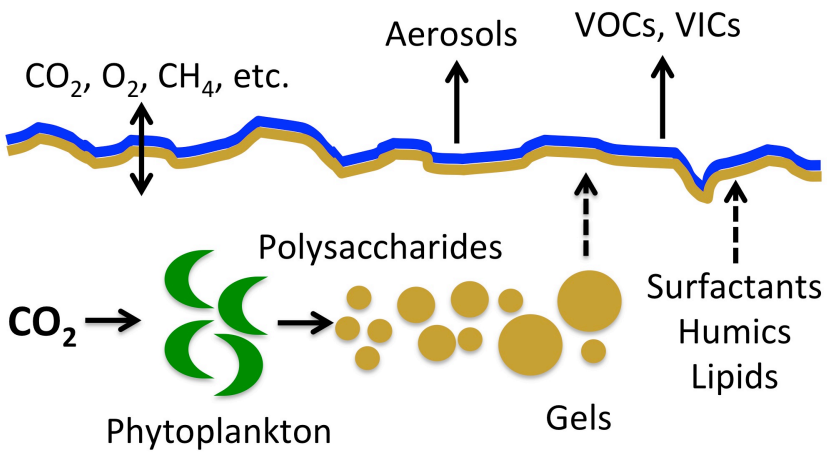

Figure 5. Model of the sea surface microlayer, showing the production of photosynthetic byproducts by phytoplankton with associated ecological interactions and subsequent aggregation into gels and concentration at the air-water interface. The microlayer also concentrates other compounds, in addition to influencing gas exchange, aerosol production, and other global cycles.[9]

The high concentration of surfactants in the microlayer may slow the rate of air-sea gas exchange under certain physical conditions.[37] Release of an artificial surfactant film in the northeast Atlantic Ocean confirmed that the presence of an artificial microlayer suppressed gas exchange rates by 25%, even in winds of 10 m s^{-1}.[37] Further modification of the exchange of O_2, CO_2, CH_4, and other gases by microbial communities present in the sea surface microlayer[9] may together significantly influence the fluxes of greenhouse gases and other volatile species to the atmosphere[10]. If the sea surface microlayer proves significant in controlling the fluxes of climate active gases over a large portion of the ocean, our models will need to be altered to account for this factor.

1.3.2 Chemical Reactions at the Air-Water Interface

The unique physical, chemical, and biological properties of the sea surface microlayer provide the potential for microlayer-specific solubilization and chemical processes.[7,9] Enrichment of surface-active and hydrophobic chemical species, particularly dissolved organic matter (DOM),

as well as its unique position at the air-sea interface, may greatly impact the rates and types of chemical reactions that occur in the sea surface microlayer.[7] Concentration of photochemical and photosensitized reactants near the ocean surface has been demonstrated to significantly enhance heterogeneous surface reactions, although the effect of organic microlayers on this process is not well understood.[7,11] Local variability in enrichment of specific organic compounds is likely to control the rate and scope of such microlayer-mediated reactions on a regional basis. Using simple organic films as a model, the sea surface microlayer is predicted to influence surface reactions in several ways: preventing interfacial transport or surface hydrolysis of gas-phase species, concentrating gas-phase reagents, or reacting directly with impinging gas-phase species to produce aqueous and gas phase products (Fig. 6).[7] The specific interaction is likely to depend on the hydrophobicity, thickness, composition, and other chemical properties of the microlayer, in addition to those of the impinging gas species and aqueous reactants.

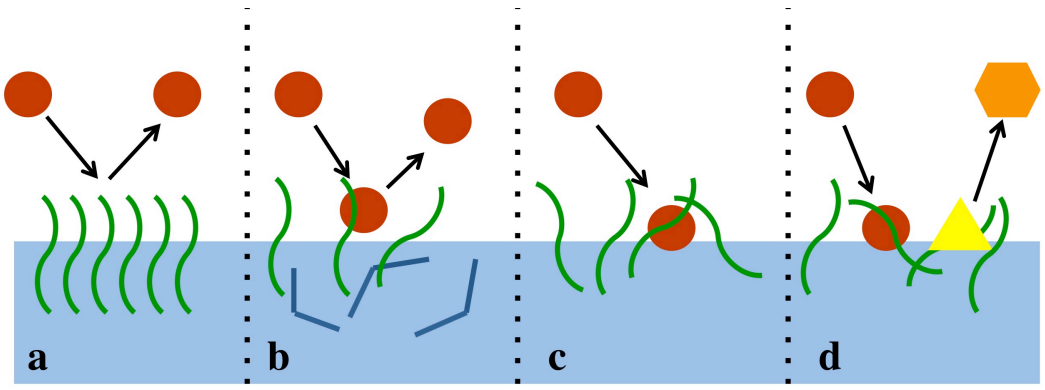

Figure 6. Proposed model for the effects of a simple organic coating on interfacial transport and chemical processes, adapted from Donaldson and George (2012).[7] The coating may (a) prevent interfacial transport of, (b) prevent surface hydrolysis of, (c) concentrate, or (d) react with the gas phase species of interest (red circles).

More specifically, the sea surface reaction between iodide and ozone, which may account for up to 75% of the observed IO levels over the tropical Atlantic[26], is likely to be strongly influenced

by microlayer composition and thickness, and thus may affect the diffusion rates of both reactants, interfacial transfer rates of ozone and gas-phase products, and surface concentrations of both species. For example, model octanol coatings have been demonstrated to alter the gas-solution partitioning of I_2 produced by the reaction between O_3 and I^-.[38] Hence, regional variability in microlayer characteristics, likely driven by the underlying biology, in addition to physical processes such as wind speed, may play a role in controlling the fluxes of ozone and iodine across the air-sea interface.

1.4 Sea Surface Reaction between Ozone and Iodide

1.4.1 Overview

The reaction between gaseous O_3 and aqueous I^- is proposed to follow one of two competing mechanisms: Langmuir-Hinshelwood, where the $O_3(g)$ is adsorbed to the surface prior to reaction, or Eley-Rideal, where the gaseous ozone reacts directly with $I^-(aq)$.[26-27,38-39] In both cases, the rate of ozone deposition is first order in $[O_3]_g$ and can be modeled by:

$$\frac{d[O_3]_g}{dt} = -\frac{S v_d [O_3]_g}{V} \tag{7}$$

where S (cm^2) is the surface area of the air-water interface, v_d ($cm\ s^{-1}$) is the ozone deposition velocity, and V (cm^3) is the volume of gas over area S.[26-27,38-39] The ozone deposition velocity is expected to be dependent on bulk ozone and iodide concentrations[26-27] and microlayer composition and concentration, as well as physical parameters of the experimental setup.

On a larger scale, the spatial and temporal variability in ozone and iodide concentrations at the air-water interface is likely to result in regional differences in the production of reactive iodine

species, as well as ozone deposition rates. Recent studies have shown that the presence of large, unsaturated biomolecules, as well as chromophoric DOM, can act to enhance ozone deposition to the sea surface, while simultaneously producing VICs.[26-27] Chlorophyll, which is released following the death of photosynthetic plankton, was used as a proxy for O_3 deposition due to DOM at the sea surface, and was found to be a significant sink of ozone, particularly in coastal regions.[6] Reactions with both I^-(aq) and DOM were required to replicate observations of IO generation, as well as ozone deposition, in climate models.[5] As a result, understanding the dominant controls on the rate and scope of the sea surface reaction between ozone and iodine is key to predicting fluxes of reactive iodine into the atmosphere and ozone into the ocean.

1.4.2 Langmuir-Hinshelwood Mechanism

Heterogeneous reactions between gaseous O_3 and liquid substrates frequently obey Langmuir-Hinshelwood mechanisms, which occur when a reaction takes place between two co-adsorbed species, one or both of which exhibits a surface concentration given by a Langmuir adsorption isotherm.[26,38-39] In such cases, the surface concentration of the species of interest, $[A]_\sigma$, is given by:

$$[A]_\sigma = \frac{[N]_\sigma^{Max} R [A]_{Bulk}}{1 + R[A]_{Bulk}} \quad (8)$$

where $[A]_{bulk}$ is the bulk-phase (aqueous or gaseous) concentration of the species of interest, $[N]_\sigma^{Max}$ is the maximum number of surface binding sites, and R is a parameter that depends on the ratio of the rate of adsorption to the surface to the sum of the rates of competing processes (desorption, diffusion, competing reactions).[38-40] The rate of such reactions is directly dependent on the concentration of both co-adsorbed species at low concentration, but inhibited by high

concentrations of either reactant.[38] The reaction rate can be expressed in terms of the bulk reactant concentrations by including a Langmuir isotherm describing the bulk-surface partitioning behavior (Eq. 8).[38] The generalized surface reaction:

$$A(g) + B(aq) \rightarrow C(aq) \tag{9}$$

where both A and B have surface concentrations given by Langmuir adsorption isotherms and the only processes affecting the surface concentrations of A and B are adsorption to and desorption from the surface layer, has a reaction rate given by:

$$\frac{d[C]_{aq}}{dt} = k_{\sigma}[A]_{\sigma}[B]_{\sigma} \tag{10}$$

where k_{σ} is the surface bimolecular rate constant, $[A]_{\sigma}$ is the surface concentration of species A, and $[B]_{\sigma}$ is the surface concentration of species B. Using Langmuir adsorption isotherms to describe $[A]_{\sigma}$ and $[B]_{\sigma}$ (Eq. 8), this can be re-written as:

$$\frac{d[C]_{aq}}{dt} = k_{\sigma}\left(\frac{[N]_{\sigma}^{Max} R[A]_{g}}{1+R[A]_{g}}\right)\left(\frac{[N]_{\sigma}^{Max} R'[B]_{aq}}{1+R'[B]_{aq}}\right) \tag{11}$$

where R is the ratio of the adsorption to desorption rate for A and R' is the ratio of the adsorption to desorption rate for B.

Sakamoto et al. (2009) used cavity ring-down spectroscopy to study the surface reaction between ozone and iodide and concluded that the production of IO(g) and I_2(g) showed Langmuir-Hinshelwood dependences on the concentrations of both O_3(g) and I^-(aq).[38-39] The observed pH-

dependence of the reaction, the assumed Langmuir-Hinshelwood mechanism, and the measurement of IO(g) as a product led to the following proposed mechanism for the reaction, where the initial ozonation of $I^-(aq)$ proceeds through an $IOOO^-_\sigma$ intermediate, in analogy to the reported $BrOOO^-$ intermediate for the reaction between ozone and Br^-.[39]

$$I^-_\sigma + O_{3,\sigma} \rightarrow IOOO^-_\sigma \quad (12)$$

$$IOOO^-_\sigma \rightarrow IO^-(aq) + O_2(aq) \quad (13)$$

$$IO^-(aq) + H^+ \leftrightarrow HOI(aq) \quad (14)$$

$$HOI(aq) + I^-(aq) + H^+ \leftrightarrow I^-(aq) + H_2O \quad (15)$$

Prior to Eq. 12, O_3 and I^- partition between the surface and bulk according to Eq. 8 and, following Eq. 15, I_2 partitions into the gas phase, in addition to reaching equilibrium with $I_3^-(aq)$ if excess $I^-(aq)$ is present (Eq. 3). The production of IO(g) is proposed to result from reactions involving the $IOOO^-_\sigma$ intermediate, I^-_σ, and HOI(aq).[39] An additional reaction with $O_3(aq)$ can compete with reaction 16 to produce $IO_3^-(aq)$:

$$HOI / IO^-(aq) + 2O_3(aq) \rightarrow IO_3^-(aq) + 2O_2(aq) + H^+ \quad (16)$$

although, as reaction 15 is faster than reaction 16, $IO_3^-(aq)$ is expected to be a minor product.[39] Reactions 12-16 are shown schematically in Fig. 7.

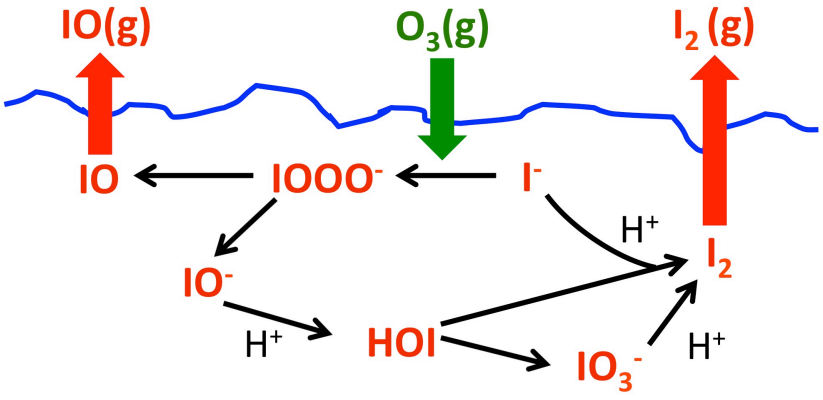

Figure 7. Proposed reaction scheme for sea surface reaction between O_3 and I^-, assuming a Langmuir-Hinshelwood mechanism.[39]

Further studies have confirmed that $I_2(g)$ production demonstrates direct dependence on both gaseous ozone[38] and aqueous iodide[27] for concentrations in the range typically seen in the tropical MBL and seawater, respectively, which provides further support for a Langmuir-Hinshelwood mechanism. The pH-dependence of this set of reactions (Eq. 14-16) indicates the predicted decrease in ocean pH over the next century might influence ozone deposition and $I_2(g)$ production in the long term.

1.4.3 Eley-Rideal Mechanism

An alternative mechanism, which is driven by fast accommodation of ozone gas in the surface microlayer, followed by direct reaction with I^-_σ, has the basic mechanism given in Eq. 17-18.

$$H^+ + I^-_\sigma + O_3(g) \rightarrow HOI(aq) + O_2(aq) \quad (17)$$

$$H^+ + HOI(aq) + I^-(aq) \leftrightarrow I_2(aq) + H_2O \quad (18)$$

In this model, the ozone deposition velocity (Eq. 7) is controlled by serial resistances that determine the movement and partitioning of ozone between the layers of the atmosphere and

surface ocean.[6,26] In the simplest case, v_d is only a function of the resistance of the aqueous phase, Γ_s, and the aerodynamic resistance of the overlying air, Γ_a:

$$v_d = \frac{1}{\Gamma_a} + \frac{1}{\Gamma_s} \tag{19}$$

$$\Gamma_s = \frac{H}{\sqrt{\lambda D}} \tag{20}$$

where H is the gas-over-liquid form of the dimensionless Henry's law constant, D ($m^2\ s^{-1}$) is the molecular diffusivity of ozone in water, and λ (s^{-1}) is the integrated first order loss of ozone in sea water.[26] Additional terms can be added to Eq. 19 to reflect transport through the quasi-laminar atmospheric boundary layer[6], as well as movement through a microlayer. The rate of $I_2(g)$ production is dependent on the $O_3(g)$ concentration, I^-_σ, surface pH, competing reactions, and the mixing rates between the surface and bulk.[6,26] The high reactivity of O_3 and I^-, as well as the high volatilization rates of evolved iodine species mean there is little competition for ozone or iodide by other reactants, and the thickness of the layer in which reactions 17-18 occur can be defined by Eq. 21.[26]

$$\delta = \sqrt{D/\lambda} \tag{21}$$

The reactions described by Eq. 17-18 are shown schematically in Fig. 8, in addition to the layer defined by Eq. 21. Measurements of gaseous HOI and I_2 emissions from ozonized iodide solutions and seawater at varying iodide concentrations were well modeled by this mechanism, which treated the interfacial layer as a box with only vertical mixing into the bulk solution or overlying air.[26]

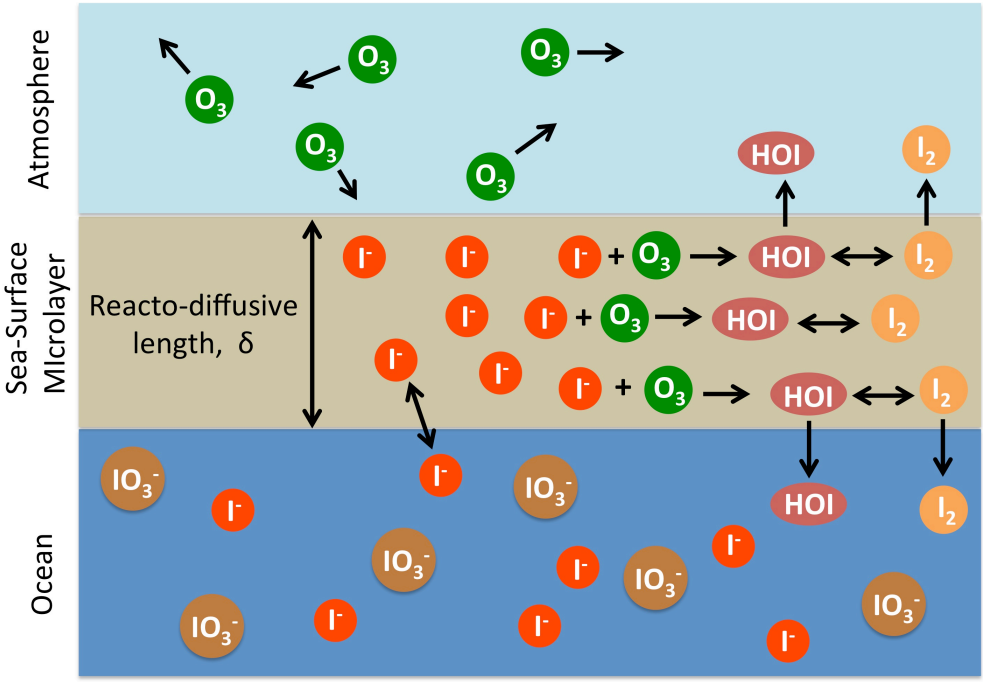

Figure 8. Schematic representation of Eley-Rideal mechanism of the sea surface reaction between ozone and iodide.[26]

1.4.4 The Sea Surface Microlayer and Ozone Deposition Mechanisms

The basic Langmuir-Hinshelwood (Eq. 8,11) and Eley-Rideal (Eq. 19-21) mechanisms describing the reaction between ozone and iodide do not include the influence of a sea surface microlayer and need to be altered to investigate such effects. In the case of the Langmuir-Hinshelwood mechanism, the number of available surface sites (Eq. 8) is expected to differ based on the composition of the microlayer as a result of differences in hydrophobic-hydrophilic interactions, surface packing density, and chemical reactivity (Fig. 6). Additionally, the reaction rates describing adsorption to and desorption from the surface layer, diffusion within the layer, and competing chemical processes within the layer may be altered by the addition of organic films to the water surface. Taken together, these effects are predicted to change the bulk-surface partitioning of the species involved in the reaction, and thus the rate of product formation (Eq.

10). Octanol films have been demonstrated to alter the gas-solution partitioning of I_2 produced from this reaction, and similar effects are expected for the reactants.[38] Analogous changes need to be made to apply the Eley-Rideal mechanism to situations when microlayers are present. In particular, the addition of a term to account for the microlayer resistance in Eq. 19, with consequent use of molecular diffusivity and chemical loss mechanisms representative of the surface microlayer (Eq. 20), is necessary. Studies examining the sea surface reaction between ozone and iodine have provided support for both proposed mechanisms,[26-27,38-39]although the scarcity and heterogeneity of global gas flux measurements with which to compare model results make confirmation difficult[1,5-6]. Most studies to date have been performed in buffered MQ water without the addition of organic films, in addition to ignoring complicating factors such as wind speed, wave breaking, and bubble formation, so extrapolation to natural systems is difficult. Comparison between studies is also hindered by the wide range of ozone and iodide concentrations used, the species measured, and the variables considered.

This work examines the role organic films may play in controlling ozone deposition velocity by adding soluble and insoluble model surfactants to bulk-phase solutions and measuring the reduction in gas phase ozone concentration following addition of iodide to the aqueous phase. Both buffered and natural seawater solutions were used, to allow the results to be more easily compared to natural systems. However, measurements of gas-phase ozone loss rates alone cannot be used to differentiate between the proposed mechanisms, since both assume first order loss of ozone from the atmosphere into the ocean surface (Eq. 7). Additional measurements of bulk-surface partitioning or direct measurements of product generation would be required to distinguish between the Langmuir-Hinshelwood and Eley-Rideal mechanisms.

2 Methods

2.1 Apparatus

The experimental apparatus used to measure ozone deposition velocities to phosphate-buffered solutions and seawater with varying iodide and surfactant concentrations was modeled after those of Martino et al. (2012) and Carpenter et al. (2013), and is shown schematically in Fig. 9.[26-27] Teflon tubing was used for all gas flow lines to minimize loss of ozone or side reactions, and all reactions were carried out in the dark to minimize photochemistry. A 3-neck, 2 L round-bottomed flask was used as the reaction chamber, with the side necks serving as the gas inlet and outlet. The center neck was fitted with Teflon tubing and a Luer-Lok tap to allow for the addition of iodide solutions to the flask. A magnetic stir-bar was placed in the bottom of the reaction chamber to ensure the bulk solutions were well mixed.

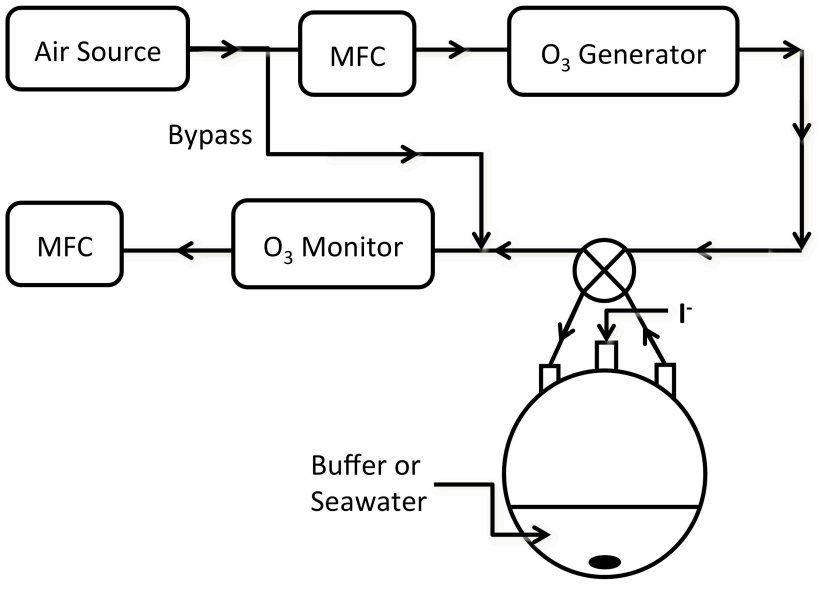

Figure 9. Schematic of experimental apparatus. Ozone was generated in situ and the concentration controlled by varying the gas flow rate using mass flow controllers (MFCs). The glass reaction vessel was covered in foil, and the Teflon tubing in black tape, to avoid photolysis during experiments.
Ozone was generated by photolysis of molecular oxygen using a mercury lamp (Eq. 4-5).

Ultrapure air was first dried (Drierite trap) and split using a needle valve. The gas flow through the ozone generator and into the reaction vessel was maintained at ~0.2 L min^{-1}, and the bypass flow at ~1.2 L min^{-1}, as determined by the requirements of the ozone analyzer. A commercial ozone generator (CAP OZN-1) was modified by the addition of a home-built quartz cell and removal of the fan. The ozone concentration was controlled by adjusting the flow rate through the ozone generator and the distance between the quartz cell and mercury lamp. Ozone concentrations were measured using a 2B Tech 205 ozone monitor, which is a dual-beam instrument that measures absorption at 254 nm in a 10 cm flow cell.

2.2 Reaction Monitoring

At the beginning of each experiment, the gas stream was delivered directly into the ozone monitor until a constant reading was established. Typical ozone concentrations used were 900-1000 ppbv. Phosphate-buffered solution (0.1 M, pH 8.0, 18 MΩ DI water) or seawater (0.2 μm filtered Sargasso surface water collected August 2013 aboard *R/V Atlantic Explorer*) was then added to the reaction vessel, and the gas stream diverted to flow through the flask. 150 mL of solution was added to the chamber for each experiment, giving a surface area S=111 cm^2 and a headspace volume V=2088 cm^3. Microlayer compounds were also added to the reaction vessel at this time: DMSO was used as a model soluble surfactant[18], stearic acid as a model insoluble surfactant[41], and alginic acid as a model microlayer gel compound[34,42-43] (Fig. 10). DMSO was added to the buffer or seawater in the reaction vessel in microliter quantities, to give bulk concentrations in the range 0.5-8 mM. Stearic acid (Sigma, 95%) was first dissolved in DMSO (Sigma, ≥99%) and then added in microliter quantities to the reaction vessel, to give bulk concentrations in the range 0.5-5 μM (1-10x monolayer coverages[41]). Alginic acid (Sigma,

sodium salt) was first dissolved in 0.2 μm filtered Sargasso SW, then mechanically ground to homogenize the gel particles, and finally added to the reaction vessel in milliliter quantities to give bulk concentrations in the range 0.3-33 μg mL^{-1}, which simulates the concentration gradient of acid polysaccharides between natural concentrations and bloom conditions.[34,42-43]

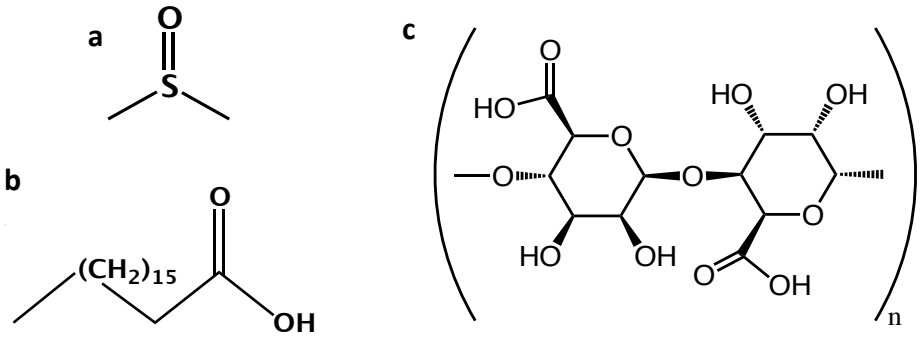

Figure 10. Structures of DMSO (a), stearic acid (b) and alginic acid (c).

After addition of phosphate buffer or seawater and microlayer compounds, the ozonized air was allowed to equilibrate with the contents of the flask for 1-2 hr, until a constant ozone reading had again been established. At this point 1 mL of iodide solution (10^{-4}-10^{-5} m NaI: Sigma, ≥99.5% in 18 MΩ DI water or 0.2 μm filtered Sargasso seawater) was added to the reaction vessel using a gas tight syringe via the Luer-Lok tap and tubing in the central neck of the flask. The bulk solution was stirred at a rate so as to ensure the bulk solution was well-mixed, but not to disturb the formation of microlayers. The gas-phase ozone concentration was monitored as a function of time, and the reaction allowed to proceed for several hours.

3 Experimental Results and Discussion

3.1 Experimental Conditions

Model microlayer compounds were chosen based on both their chemical properties and applicability to natural marine systems. DMSO is a degradation product of DMS, a biogenic gas that is present globally in marine surface waters and impacts climate through exchange with the atmosphere.[44] The concentration of DMSO in surface waters often exceeds that of DMS and its precursor, DMSP, and concentrations up to 60 nM have been measured in the Ross Sea.[44]As a result of its ubiquity in the surface ocean[44] and surface active properties,[18,45-46] DMSO was chosen as a model water-soluble surfactant. Because of its solubility, a monolayer coverage of DMSO requires significantly higher than natural concentrations (>7 M),[46] and so concentrations in the range 0.5-8 mM were chosen as a compromise. Fatty acids, a major component of lipids, concentrate in the sea surface microlayer, and are often of biogenic origin.[47] Monolayers of stearic acid, an unsaturated fatty acid, have been shown to physically inhibit the production of gas-phase NO_2 from photolysis of aqueous NO_3^- solutions, and so it was chosen as a model water-insoluble surfactant.[41] Stearic acid was added to bulk solutions in concentrations corresponding to 1-10x monolayer coverages.[41] Alginic acid is an acid polysaccharide that aggregates into gels in aqueous environments and is produced naturally in the marine environment by brown algae.[42] The underlying structure of the sea surface microlayer is comprised primarily of a hydrated gelatinous polysaccharide matrix,[9,34] and so alginic acid was chosen as a proxy for naturally occurring microlayers in the marine environment. Bulk concentrations of alginic acid used were in the range 0.3-33 μg mL^{-1}, which simulates the natural concentration gradient between oligotrophic concentrations and bloom conditions.[34,42-43]

The physical setup of the apparatus was designed to optimize signal to noise in the widest range of iodide concentrations. The bypass flow rate, ~1.2 L min^{-1}, was determined by the requirements of the ozone monitor. High ozone (900-1000 ppbv) and iodide concentrations (2-10 μM) were required so that the decrease in ozone concentration due to the reaction was significantly larger than the detection limit of the instrument. Low flow rates through the reaction vessel (~0.2 L min^{-1}) and a large headspace volume (2088 cm^3) ensured the residence time was long enough (~10 min) that the surface layer could become saturated with ozone and the reaction would occur quickly after the addition of iodide to the flask. Additional sensitivity can be gained with lower ozone and iodide concentrations by changing the reaction vessel geometry. A larger signal can be obtained by increasing the surface area available for the reaction to occur in while retaining a large headspace volume, which may also allow these reactions to be conducted with ozone and iodide concentrations closer to those of natural marine systems. Alternatively, reducing the flow rate required by the ozone monitor will also decrease the detection limit and thus the concentrations of reactants required for an acceptable signal to noise ratio.

3.2 Modeling Ozone Deposition

The ozone deposition velocity was calculated using a mass-flux based model in two stages. The first stage was to determine the steady state O_3 concentration in the reaction vessel in the presence of bulk solution and microlayer compounds (if present) and absence of iodide, with the flask contents assumed to serve as a sink of unknown magnitude. Eq. 22 was fit to each dataset using least squares nonlinear regression to optimize $\Delta[O_3]_g$, the difference between the concentration of ozone entering the flask, $[O_3]_g^0$, and the concentration leaving the flask, $[O_3]_g$:

$$\frac{d[O_3]_g}{dt} = \frac{F([O_3]_g^0 - \Delta[O_3]_g)}{V} - \frac{F[O_3]_g}{V} \quad (22)$$

where F is the gas flow rate through the flask (L min^{-1}), V is the headspace volume of the flask (2.088 L), and ozone concentrations were measured in ppbv.[48] In this simple model, the flow rates entering and exiting the flask are equivalent (F) and the headspace volume is constant, so the steady-state ozone concentration will approach $[O_3]_g^0 - \Delta[O_3]_g$. This means $\Delta[O_3]_g$ represents the magnitude of the ozone loss caused by interaction with the reaction vessel, bulk solution, and any microlayer compounds present. Measured values of $\Delta[O_3]_g$ were slightly larger in seawater than phosphate-buffered solutions, and were within the range of 3-15% of the ozone concentration entering the flask.

The second stage was used to model the reaction, assuming the loss rate of gaseous ozone is first order in $[O_3]_g$.[26-27,38-39] Eq. 23 was fit to the data using nonlinear least squares regression to optimize v_d, the ozone deposition velocity:

$$\frac{d[O_3]_g}{dt} = \frac{F([O_3]_g^0 - \Delta[O_3]_g)}{V} - \frac{F[O_3]_g}{V} - \frac{Sv_d[O_3]_g}{V} \quad (23)$$

where S (111 cm^2) is the surface area of the solution inside the reaction vessel, and using the optimized value of $\Delta[O_3]_g$ as a constant.[48] Example traces showing FFT-filtered data with the modeled fits using Eq. 22 and 23 overlaid are shown for a sample with no added microlayer (Fig. 11a) and a sample with a stearic acid concentration of 4.93 μM (Fig. 11b). The model fits the data well in both cases, and the rate of ozone loss as a result of the reaction with I^- is clearly

decreased by the presence of stearic acid. This also verifies that the decrease in gas phase ozone can be accurately represented by a first order loss term (Eq. 7).

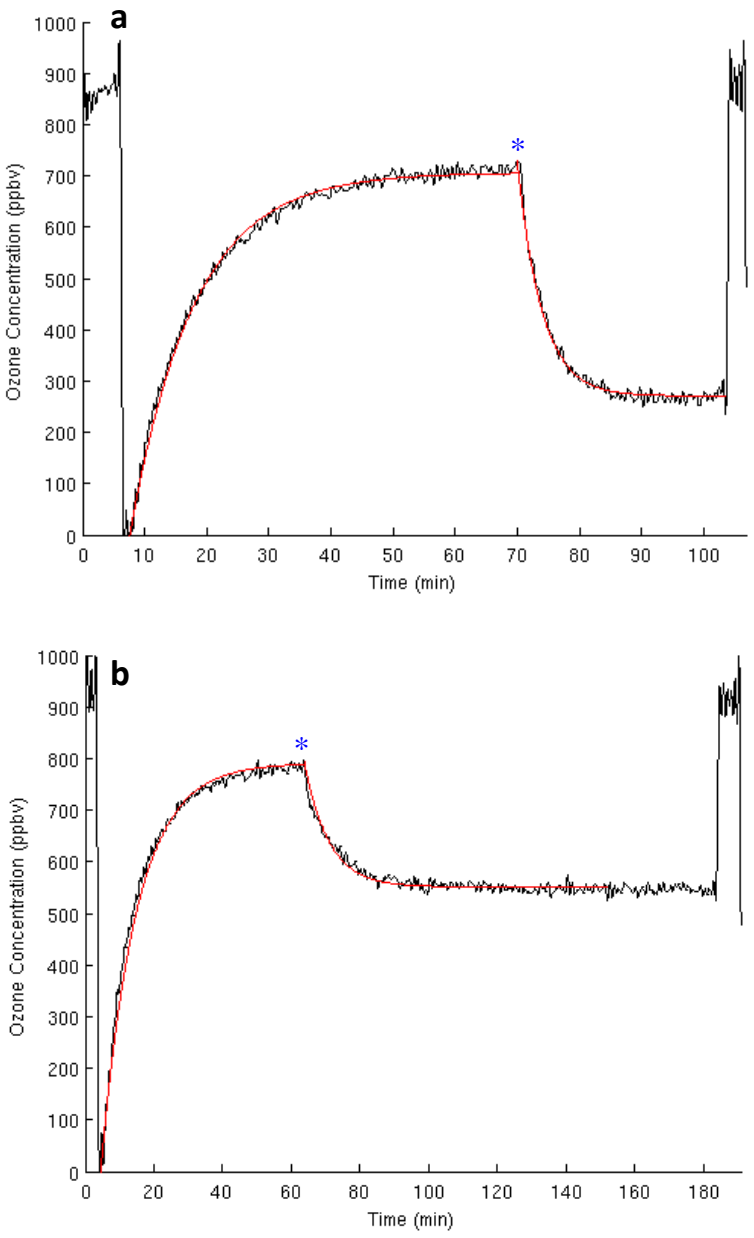

Figure 11. Example traces showing the time-dependence of ozone concentration throughout an experiment (black) and the fitted model (red), with the addition of iodide marked by a blue star. The initial decrease was caused by switching the flow from the bypass to the reaction vessel, the second decrease was caused by the addition of I^-, and the final increase is a result of switching the flow back to the bypass. Both traces were collected at an iodide concentration of 5 μM and 0.2 μm-filtered Sargasso seawater as the solvent; (a) had no added microlayer and (b) had 4.93 μM stearic acid added.

3.3 Influence of Organic Microlayers on Ozone Deposition

The influences of iodide concentration, microlayer composition, and surfactant concentration on ozone deposition velocities were examined using DMSO as a model soluble surfactant[18], stearic acid as a model insoluble surfactant[41], and alginic acid as a model gel compound[34,42-43], which represents the majority of the sea surface microlayer in most cases[9] (Fig. 10). Ozone deposition velocities and associated uncertainties are given in Table A1 (Appendix A) for experiments conducted with and without surfactants, in phosphate-buffered solutions and seawater, and at varying iodide concentrations. Uncertainties were estimated from the variance of the nonlinear fits to Eq. 23.[48] A summary of linear regression coefficients, uncertainties, and p-values for datasets, when applicable, is given in Table A2 (Appendix A).

The impact of iodide concentration on ozone deposition velocity in the absence of a microlayer is shown in Fig. 12. Deposition velocities measured in seawater exhibited a linear relationship with $[I^-]_{bulk}$, as expected based on previous studies,[27,39] and were lower than the corresponding deposition velocities measured in phosphate-buffered solution. This is likely due to differences in activity coefficients between phosphate-buffered solutions and seawater, or the presence of small amounts of natural DOM.[5-6,26-27,31]

A linear relationship between ozone deposition velocity and $[I^-]_{bulk}$ is also seen for additions of alginic acid to seawater (Fig. 13), and the deposition velocities for samples with alginic acid additions are the same as those without, within the estimated uncertainties (Fig. 14). This indicates either the addition of alginic acid had little impact on the flux and partitioning of ozone into the sea surface or, more likely, the method of sample preparation did not accurately mimic the formation of natural microlayers.

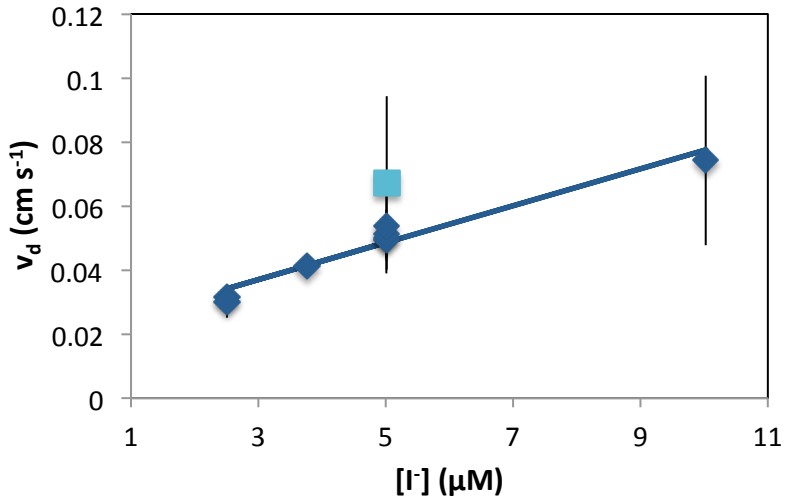

Figure 12. Ozone deposition velocity as a function of [I^-] for experiments with no added microlayer. Experiments were conducted using both phosphate-buffered deionized water (light blue squares) and 0.2 μm-filtered Sargasso seawater (dark blue diamonds) as the solvent. Linear regression coefficients and statistics are given in Table A2 (Appendix A).

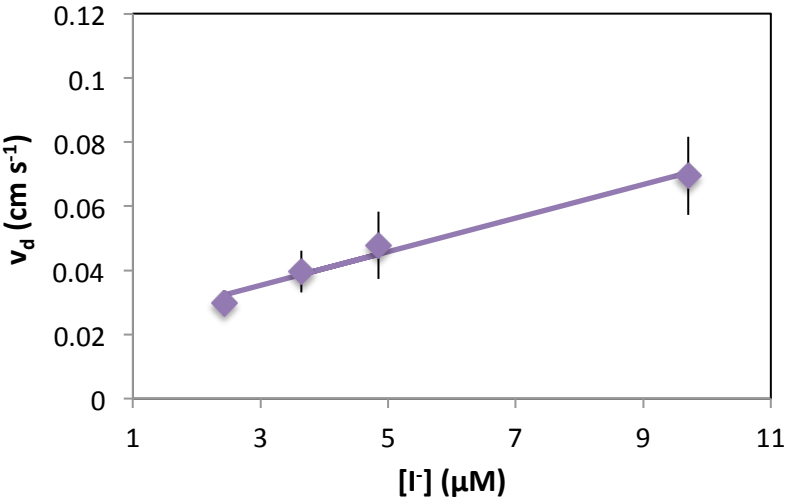

Figure 13. Ozone deposition velocity as a function of [I^-] for experiments with varying additions of alginic acid. Experiments were conducted with a bulk alginic acid concentration of 32.6 μg mL^{-1} in 0.2 μm-filtered Sargasso seawater. Linear regression coefficients and statistics are given in Table A2 (Appendix A).

Ozone deposition velocities to seawater as a function of iodide concentration are given in Fig. 14 for experiments conducted with and without additions of DMSO, stearic acid, or alginic acid. As observed in Fig. 12-13, the relationship between ozone deposition velocity and iodide

concentration is linear for samples without microlayers or with alginic acid additions. Deposition velocities measured at the same iodide concentration for samples without microlayers or with alginic acid or DMSO additions agree within the estimated uncertainty. This indicates that, at least within the concentration range studied, DMSO has a negligible effect on the flux or partitioning of ozone into the sea surface. By contrast, the addition of stearic acid is seen to decrease ozone deposition velocities at all iodide concentrations. This suggests stearic acid is acting to reduce the flux of ozone across the sea-air interface, as has been observed for other water-insoluble organic coatings in both the laboratory and ocean.[8,37-38]

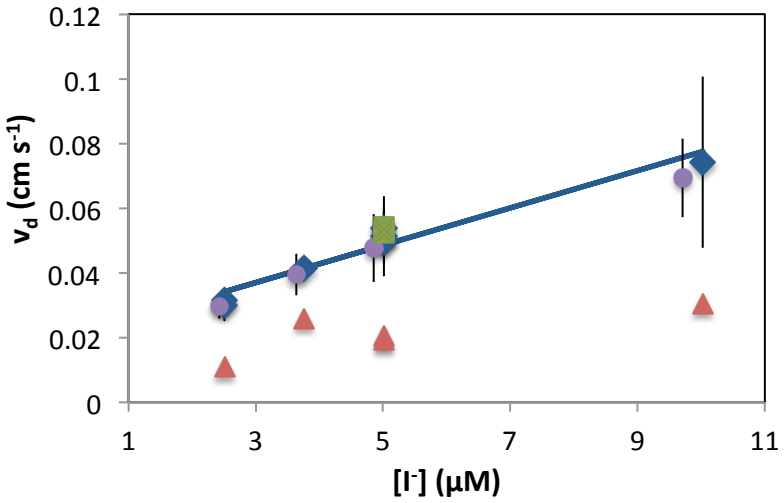

Figure 14. Ozone deposition velocity as a function of [I^-] for experiments with varying microlayer composition. Experiments were conducted using 0.2 μm-filtered Sargasso seawater as the solvent, with no added microlayer (dark blue diamonds), 2.47 μM stearic acid (red triangles), 32.6 μg mL^{-1} alginic acid (purple circles) or 4.03 mM DMSO (green squares). Linear regression coefficients and statistics are given in Table A2 (Appendix A).

The influence of microlayer composition and surfactant concentration on ozone deposition velocity was also examined using 5 μM iodide concentrations. The results are shown in Fig. 15 for DMSO, where experiments were conducted in both phosphate-buffered solutions and seawater. Measured deposition velocities decreased slightly, but significantly, with increasing

DMSO concentration for experiments using phosphate buffer as the solvent, but exhibited no significant trend for experiments conducted in seawater. This may result from differences in microlayer formation mechanism or efficiency in solutions with varying ionic strength. In particular, the bulk-surface partitioning of organic compounds in solution is altered by the addition of salt; the effect is to increase the surface concentration relative to the bulk.[49] Additionally, deposition velocities measured in phosphate-buffered solution were consistently higher than those measured in seawater, as was observed for experiments conducted without surfactant additions (Fig. 12). This difference is again attributed to differences in activity coefficients, or the presence of small amounts of natural DOM.[5-6,26-27,31]

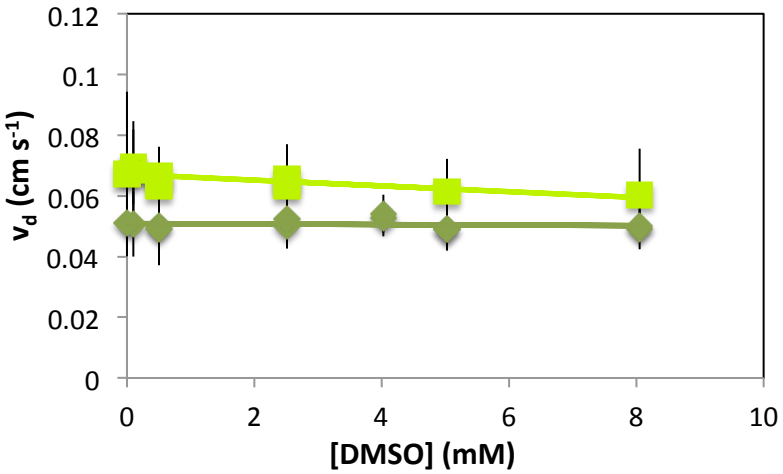

Figure 15. Ozone deposition velocity as a function of DMSO concentration. Experiments were conducted using 5 μM I^- and either phosphate-buffered deionized water (light green squares) or 0.2 μm-filtered Sargasso seawater (dark green diamonds) as the solvent. Linear regression coefficients and statistics are given in Table A2 (Appendix A).

A similar relationship as for DMSO was obtained between ozone deposition velocity to seawater and alginic acid concentration (Fig. 16). No significant trend was observed, and the measured ozone deposition velocities at all alginic acid concentrations agreed within experimental uncertainty with the results obtained in the absence of a microlayer. Multiple linear regression

using iodide concentration and alginic acid concentration as independent variables confirmed that iodide concentration was the only significant factor in determining ozone deposition velocities.

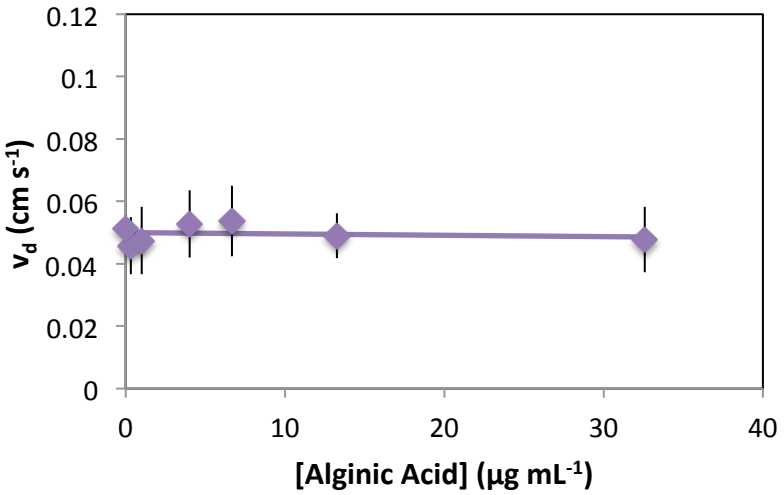

Figure 16. Ozone deposition velocity as a function of alginic acid concentration. Experiments were conducted using 5 µM I^- and 0.2 µm-filtered Sargasso seawater as the solvent. Linear regression coefficients and statistics are given in Table A2 (Appendix A).

The influence of stearic acid additions to both phosphate-buffered solutions and seawater on ozone deposition velocity is shown in Fig. 17. Ozone deposition velocity initially decreased quickly with increasing stearic acid concentration, but leveled off around 4-5 µM stearic acid. The effect of stearic acid appears to be independent of the bulk solution; deposition velocities measured in both phosphate buffer and seawater agree to within their respective uncertainties.

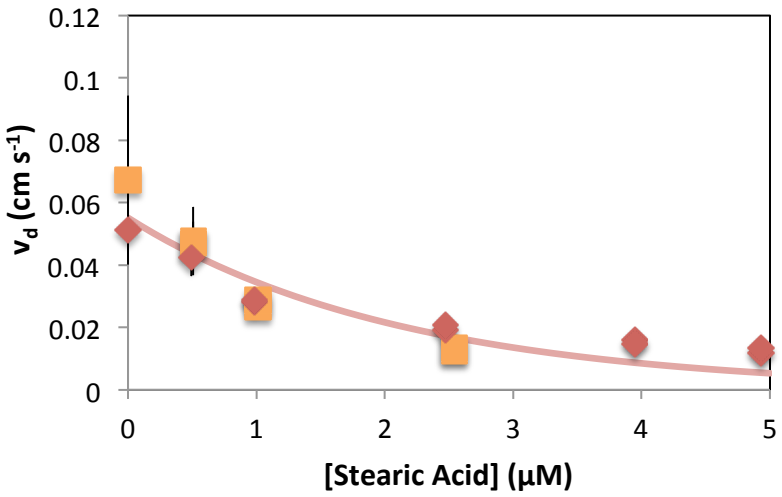

Figure 17. Ozone deposition velocity as a function of stearic acid concentration. Experiments were conducted using 5 μM I^- and either phosphate-buffered deionized water (orange squares) or 0.2 μm-filtered Sargasso seawater (red diamonds) as the solvent. A least squares exponential fit to both data sets of the form $Ae^{-k[SA]}$ gave $A = 0.0551 \pm 0.0034$ and $k = 0.467 \pm 0.063$.

Least squares exponential regression was used to fit the composite data of Fig. 17 to a function of the form $Ae^{-k[SA]}$, where [SA] is the stearic acid concentration and A and k are the variables optimized by regression. Nonlinear least squares regression was then used to determine the equation of the surface best describing the relationship between ozone deposition velocity, iodide concentration, and stearic acid concentration (Table A1, Appendix A), assuming a linear relationship between iodide and deposition velocity (Fig. 12) and an exponential relationship between stearic acid concentration and deposition velocity (Fig. 17).[48] The surface shown in Fig. 18 describes these relationships, and is given by:

$$v_d = m[I^-]_{bulk} + Ae^{-k[SA]} + b \qquad (24)$$

where $m = 0.0021 \pm 0.0009$, $A = 0.0467 \pm 0.0036$, $k = 0.9838 \pm 0.1931$, and $b = 0.0030 \pm 0.0051$. The good agreement between the modeled surface and experimental data (Fig. 18) indicates that both iodide and stearic acid concentration strongly influence ozone deposition velocities, and so

regional variability in iodide concentration, microlayer composition, or surfactant concentration may be predicted to impact ozone gas fluxes into the ocean surface.

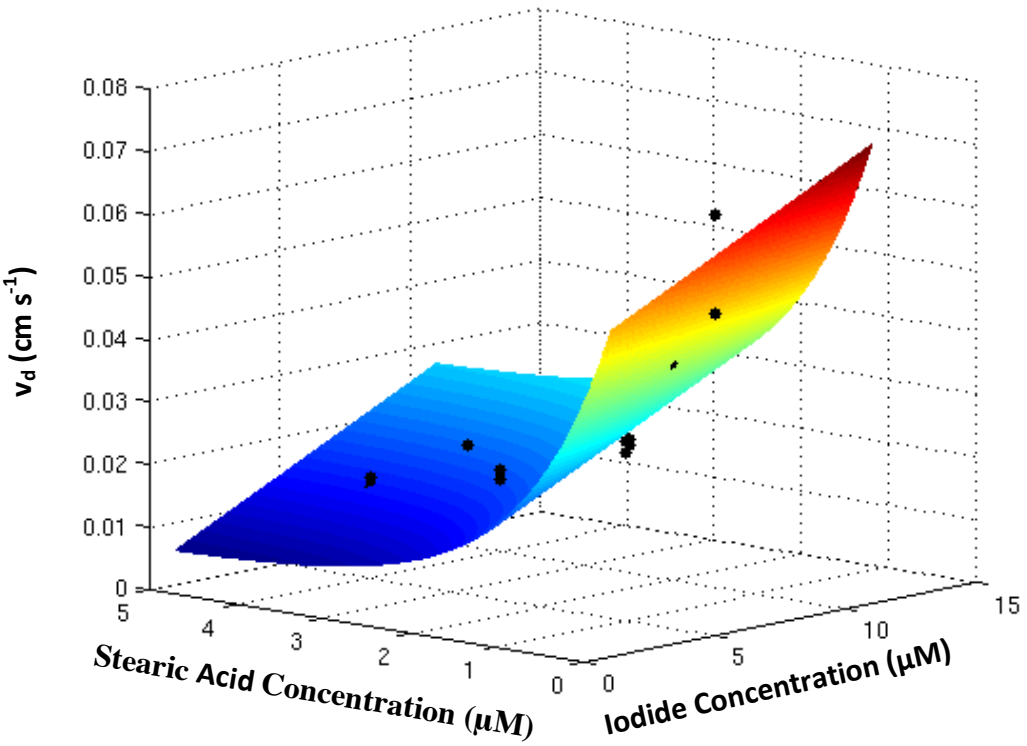

Figure 18. Surface representing the relationship between stearic acid concentration, iodide concentration, and ozone deposition velocity (Eq. 24). The magnitude of the predicted ozone deposition velocity is depicted by the colored surface, and the experimental data shown as black dots.

4 Conclusions and Future Directions

Measured deposition velocities were in the range 0.0298±0.0040 cm s^{-1} to 0.074±0.026 cm s^{-1} for experiments with no added microlayer or additions of alginic acid or DMSO, and in the range 0.0109±0.0014 cm s^{-1} to 0.0424±0.0059 cm s^{-1} for additions of stearic acid, which are all within the expected range measured over the ocean (0.01-0.1 cm s^{-1}) despite the higher concentrations of iodide and ozone used in this experiment.[27] These deposition velocities measure only the effect of added iodide and microlayer compounds and exclude the physical influences of

turbulence and wind speed; although stirring the solution may potentially enhance ozone deposition velocities, it affects all stages of the experiment in the same manner and so the measured v_d should be independent of this effect.[27] Similar laboratory experiments performed with natural seawater report ozone deposition velocities in the range 0.03-0.05 cm s^{-1}.[31] Deposition velocities measured with addition of stearic acid microlayers were significantly lower than this, despite being at higher iodide and ozone concentrations, which indicates that concentration of water-insoluble organics in the sea surface microlayer may have a significant influence on ozone deposition rates. Because such compounds are primarily biogenic in origin, this effect is likely to be coupled to the seasonal variability in underlying phytoplankton and bacterial ecology.

Iodide concentration also exhibited a significant influence on ozone deposition velocity (Fig. 12-14,18) and so regional variability in iodide concentration is expected to play a major role in controlling the sea-air flux of ozone and VICs. The concentration and speciation of aqueous-phase iodine species, like many fatty acids and other water-insoluble organics, is driven in large part by the density, species, and life-cycle stage of planktonic phytoplankton and bacteria, and in coastal regions, macroalgae.[15-17] As a result, understanding the spatial and temporal heterogeneity in the fluxes of both ozone and iodine across the sea-air interface will require knowledge of interaction between chemistry and biology on a regional scale.

More accurate models of sea-air gas fluxes will also require explicit consideration of the effects of wind speed, bubble bursting, and wave action. The impact of these processes on the physical mechanism of microlayer formation is an area of active study,[10,30,33,37] but the implications for microlayer chemistry is less well understood[7,38,41]. Additional studies integrating these physical

effects with the chemical influences of the sea surface microlayer are required to fully understand air-sea exchange of reactive trace gases. Furthermore, experiments conducted with alternative model surfactants, more natural microlayer proxies, and those exploring the role of photochemistry in ozone deposition are also needed. Another area of potential interest is the impact of pH changes on the surface reaction between ozone and iodide, as well as competing reactions. The rate of the reaction between ozone and iodide has been shown to be pH-dependent,[26,39] and so the predicted decrease in ocean pH over the next century may also influence ozone and VIC gas fluxes, and thus tropospheric chemistry and radiative forcing.

References

1. Myhre, G., D. Shindell, F.M. Bréon, W. Collins, J. Fuglestvedt, J. Huang, D. Koch, J.-F. Lamarque, D. Lee, B. Mendoza, T. Nakajima, A. Robock, G. Stephens, T. Takemura and H. Zhang, 2013: Anthropogenic and Natural Radiative Forcing. In: Climate Change 2013: The Physical Science Basis. Contribution of Working Group I to the Fifth Assessment Report of the Intergovernmental Panel on Climate Change [Stocker, T.F., D. Qin, G.K. Plattner, M. Tignor, S.K. Allen, J. Boschung, A. Nauels, Y. Xia, V. Bex and P.M. Midgley (eds.)]. Cambridge University Press, Cambridge, United Kingdom and New York, NY, USA.
2. Ground-Level Ozone in the 21st Century: Future Trends, Impacts, and Policy Implications. *RSC Science Policy Report*. RSC, 2008.
3. Platt, U. Introduction to Surface Ocean-Lower Atmosphere Processes. In: AGU Geophysical Monograph 187: *Surface Ocean-Lower Ocean Processes*; Le Quere, C., and Saltzman, E., Ed.; AGU, **2009**, 3-15.
4. Saiz-Lopez, A.; Plane, J. M. C.; Baker, A. R.; Carpenter, L. J.; von Glasow, R.; Gomez Martin, J. C.; McFiggans, G.; Saunders, R. W. ACS Chem. Reviews. **2012a**, *112*, 1773-1804.
5. Saiz-Lopez, A.; Lamarque, J.F.; Kinnison, D.E.; Tilmes, S.; Ordonez, C.; Orlando, J.J.; Conley, A.J.; Plane, J.M.C.; Mahajan, A.S.; Santos, G.S.; Atlas, E.L.; Blake, D.R.; Sander, S.P.; Schauffler, S.; Thompson, A.M.; Brasseur, G. *Atmos. Chem. Phys.* **2012b**, *12*, 3939-49.
6. Ganzeveld, L.; Helmig, D.; Fairall, C.W.; Hare, J.; Pozzer, A. *Glob. Biogeochem. Cycle*. **2009**, *23*(4), GB4021.
7. Donaldson, D.J. and George, C. *Environ. Sci. Tech.* **2012**, *46*(19).
8. Liss, P. S. and Duce, R. A. The Sea Surface and Global Change. *Cambridge University Press*, **1997**.
9. Cunliffe, M. and Murrell, J.C. *ISME Journal*. **2009**, *3*, 1001-1003.
10. Wurl, O.; Wurl, E.; Miller, L.; Johnson, K.; Vagle, S. *Biogeosciences*. **2011**, *8*, 121–135.
11. Jammoul, A.; Gligorovski, S.; George, C.; D'Anna, B. *J. Phys. Chem. A*. **2008**, *112*, 1268-76.
12. Read, K.A.; Mahajan, A.S.; Carpenter, L.J.; Evans, M.J.; Faria, B.V.E,; Heard, D.E.; Hopkins, J.R.; Lee, J.D.; Moller, S.J.; Lewis, A.C.; Mendes, L.; McQuaid, J.B. Oetjen, H.; Saiz-Lopez, A. Pilling, M.J.; Plane, J.M.C. *Nature*. **2008**, *453*, 1232-35.
13. Chang, W.; Heikes, B.G.; Lee, M. *Atmospheric Environment*. **2004**, *38*, 1053-59.
14. Garland, J.A.; Elzerman, A.W.; Penkett, S.A. *J. Geophys. Res.* **1980**, ***85***, 7488-92.
15. Saunders, R.W; Saiz-Lopez, A. Iodine in the Air: Origin, Transformation and Exchange to Mammals. In *Comprehensive Handbook of Iodine*; Preedy, V., Burrow, G.N., Watson, R.R., Ed.; Elsevier, **2009**, 75-80.
16. Amachi, S. *Microbes Environ*. **2008**, *23*(4), 269-276.
17. Kupper, F. C.; Feiters, M. C.; Olofsson, B.; Kaiho, T.; Yanagida, S.; Zimmerman, M. B.; Carpenter, J. J.; Luther, G. W.; Lu, Z.; Jonsson, M.; Kloo, L. *Angew. Chem. Int. Ed.* **2011**, *50*, 11598-11620.
18. Wren, S. N.; Donaldson, D.J. *Phys. Chem. Chem. Phys.* **2010**, *12*, 2648-2654.
19. Lovelock, J.E. *Nature*. **1975**, *256*, 193-4.
20. Vogt, R., Sander, R., von Glasow, R., and Crutzen, P. J. *J. Atmos. Chem.* **1999**, *32*, 375–95.
21. Archer, S.D; Goldson, L.E.; Liddicoat, M.I.; Cummings, D.G.; Nitingale, P.D. *J. Geophys. Res.-Oceans*. **2007**, *112*.
22. Jones, C.E.; Carpenter, L.J. *Geophys. Res. Lett.* **2007**, *34*.
23. Moore, R.M.; Zafiriou, O.C. *J. Geophys. Res.-Atmos.* **1994**, *99*, 16415-420.

24. McFiggans, G.; Bale, C. S. E.; Ball, S. M.; Beames, J. M.; Bloss, W. J.; Carpenter, L. J.; Dorsey, J.; Dunk, R.; Flynn, M. J.; Furneaux, K. L.; Gallagher, M. W.; Heard, D. E.; Hollingsworth, A. M.; Hornsby, K.; Ingham, T.; Jones, C. E.; Jones, R. L.; Kramer, L. J.; Langridge, J. M.; Leblanc, C.; Lecrane, J.-P.; Lee, J. D.; Leigh, R. J.; Longley, I.; Mahajan, A. S.; Monks, P. S.; Oetjen, H.; Orr-Ewing, A. J.; Plane, J. M. C.; Potin, P.; Shillings, A. J. L.; Thomas, F.; von Glasow, R.; Wada, R.; Whalley, L. K.; Whitehead, J. D. *Atmos. Chem. Phys.* **2010**, *10*, 2975-99.
25. Ordonez, C.; Lamarque, J.F.; Tilmes, S.; Kinnnison, D.E.; Atlas, E.L.; Blake, D.R.; Santos, G.S.; Brasseur, G. Saiz-Lopez, A. *Atmos. Chem. Phys.* **2012**, *12*, 1423-47.
26. Carpenter, L. J.; MacDonald, S. M.; Shaw, M. D.; Kumar, R.; Saunders, R. W.; Parthipan, R.; Wilson, J.; Plane, J. M. C. Nature Geoscience. **2013**, *6*, 108-111.
27. Martino, M., Leze, B., Baker, A.R., Liss, P.S. *Geophys. Res. Lett.* **2012**, *39*, L50809.
28. Ganzeveld, L. N.; Lelieveld, J.; Dentener, F. J.; Krol, M. C.; Roelofs, G. J. *J. Geophys. Res.* **2002**, *107*(D16), ACH8-1 – 8-21.
29. Chameides, W. L.; Davies, D. D. *J. Geophys. Res.* **1980**, *85*, 7383-7398.
30. Jones, C.E.; Hornsby, K.E.; Sommariva, R.; Dunk, R.M,; Von Glasow, R.; McFiggans, G.; Carpenter, L.J. *Geophys. Res. Lett.* **2010**, *37*.
31. Garland, J.A.; Curtis, H. *J. Geophys. Res.* **1981**, *86*, 3183-86.
32. Sieburth, JM. **1983.** In: Cunliffe, M. and Murrell, J.C. *ISME Journal*. **2009**, *3*, 1001-1003.
33. Archer, C. L. and Jacobson, M. Z. *J. Geophys. Res.* **2005**, *110*, D12110.
34. Verdugo, P.; Alldredge, A. L.; Azam, F.; Kirchman, D. L.; Passow, U.; Santschi, P. H. *Marine Chem.* **2004**, *92*, 67-85.
35. Leck, C. and Bigg, E.K. *Tellus.* **2005**, *57B*, 305-316.
36. Wurl, O. and Holmes, M. *Mar. Chem.* **2008**, *110*, 89-97.
37. Salter, M.E.; Upstill-Goddard, R.C.; Nightingale, P.D.; Archer, S.D.; Blomquist, B.; Ho, D.T.; Huebert, B.; Schlosser, P.; Yang, M. *J. Geophys. Res.-Oceans.* **2011**, *116*, C11016.
38. Reeser, D. I. and Donaldson, D. J. *Atmos. Environ.* **2011**, *45*, 6116-6120.
39. Sakamoto, Y.; Yabushita, A.; Kawasaki, M.; Enami, S. *J. Phys. Chem. A.* **2009**, *113*(27), 7707-7713.
40. Shattuck, T. W. *Physical Chemistry-CH341*; Academx: Sagamore Beach, MA, 2012; pp 187-191.
41. Reeser, D. I.; Kwamena, N. O.; Donaldson, D.J. *J. Phys Chem C.* **2013**, *117*(43), 22260-67.
42. Thornton, D.C.; Fejes, E. M.; DiMarco, S. F.; Clancy, K. M. *Limnol. Oceanogr: Methods.* **2007**, *5*, 73-87.
43. Passow, U. Alldredge, A. L. *Limnol. Oceanogr.* **1995**, *40*(7), 1326-35.
44. Del Valle, D. A.; Kieber, D. J.; Toole, D. A.; Bisgrove, J.; Kiene, R. P. *Deep-Sea Res. I.* **2009**, *56*, 166-177.
45. Karpovich, D. S.; Ray, D. *J. Phys Chem B.* **1998**, *102*(4), 649-652.
46. Allen, H. C.; Gragson, D. E.; Richmond, G. L. *J. Phys Chem B.* **1999**, *103*(4), 660-666.
47. Zhou, S.; Gonzalez, L.; Leithead, A.; Finewax, Z.; Thalman, R.; Vlasenko, A.; Vagle, S.; Miller, L. A.; Li, S. M.; Bureekul, S.; Furutani, H.; Uematsu, M.; Volkamer, R.; Abbatt, J. *Atmos. Chem. Phys.* **2014**, *14*, 1371-1384.
48. MATLAB and Optimization Toolbox Release 2012b, the MathWorks, Inc., Natick, Massachusetts, United States.
49. Demou, E.; Domaldson, D. J. *J. Phys Chem A.* 2002, *106*(6), 982-987. Instill

Appendix A

Table A1. Measured ozone deposition velocities and uncertainties at varying iodide concentrations, surfactant concentrations, and solvents. Stearic acid concentrations are reported in μM, DMSO concentrations in mM, and alginic acid concentrations in μg mL^{-1}.

ML Compound	Solvent	ML Compound Bulk Concentration	$[I^-]$ (μM)	v_d (cm/s)	σ_{vd} (cm/s)
None	Phosphate Buffer	0	5.02	0.067	0.027
	Seawater	0	5.01	0.0495	0.0057
		0	5.01	0.0501	0.0071
		0	5.01	0.051	0.012
		0	5.01	0.0538	0.0052
		0	2.51	0.0316	0.0026
		0	3.76	0.0413	0.0033
		0	10.03	0.074	0.026
		0	2.51	0.0301	0.0049
Stearic Acid	Phosphate Buffer	0.507	5.01	0.048	0.011
		0.507	5.01	0.0470	0.0069
		1.01	5.01	0.0267	0.0029
		1.01	5.01	0.0287	0.0035
		2.54	5.01	0.0133	0.0007
		2.54	5.01	0.0125	0.0014
		2.54	5.01	0.0133	0.0007
		2.54	5.01	0.0125	0.0014
	Seawater	0.493	5.01	0.0424	0.0059
		0.986	5.01	0.0282	0.0018
		0.986	5.01	0.0289	0.0033
		2.47	5.01	0.0192	0.0009
		2.47	5.01	0.0206	0.0013
		2.47	2.51	0.0109	0.0014
		2.47	3.76	0.0258	0.0019
		2.47	10.03	0.0304	0.0023
		3.95	5.01	0.0161	0.0013
		3.95	5.01	0.0146	0.0012
		4.93	5.01	0.0118	0.0005
		4.93	5.01	0.0133	0.0009

DMSO	Phosphate Buffer	0.100	5.02	0.068	0.016
		0.100	5.02	0.070	0.012
		0.503	5.02	0.063	0.013
		0.503	5.02	0.0667	0.0094
		2.52	5.01	0.066	0.011
		2.52	5.01	0.063	0.012
		5.03	5.01	0.061	0.011
		8.05	5.01	0.060	0.015
	Seawater	0.100	5.01	0.051	0.011
		0.503	5.01	0.050	0.010
		0.503	5.01	0.049	0.012
		2.52	5.01	0.0500	0.0075
		2.52	5.01	0.0523	0.0069
		4.03	5.01	0.0525	0.0058
		4.03	5.01	0.0541	0.0062
		5.03	5.01	0.0492	0.0071
		5.03	5.01	0.0489	0.0068
		8.05	5.01	0.0493	0.0068
		8.05	5.01	0.0500	0.0035
Alginic Acid	Seawater	0.340	5.01	0.0458	0.0092
		1.01	5.01	0.047	0.011
		4.02	4.99	0.053	0.011
		6.68	4.98	0.054	0.011
		13.3	4.95	0.0490	0.0072
		32.6	2.43	0.0298	0.0039
		32.6	4.85	0.048	0.011
		32.6	3.64	0.0396	0.0064
		32.6	9.71	0.069	0.012

Table A2. Least squares linear regression coefficients, uncertainties, and p-values for those datasets to which linear regression was applied. Slopes and intercepts for regressions as a function of iodide concentration are given in cm s^{-1} μM^{-1}, those as a function of alginic acid concentration are given in cm mL s^{-1} μg^{-1}, and those as a function of DMSO concentration are given in cm s^{-1} mM^{-1}.

ML Compound	Variable	Solvent	Slope	Intercept	R^2	p-value
None	$[I^-]$	Seawater	$(5.77\pm0.54) \times 10^{-3}$	0.0197±0.0029	0.94	< 0.01
Alginic Acid	$[I^-]$	Seawater	$(5.24\pm0.51) \times 10^{-3}$	0.0195±0.0030	0.98	< 0.01
	[Alginic Acid]	Seawater	$(-4\pm11) \times 10^{-5}$	0.0500±0015	0.03	0.7
DMSO	[DMSO]	Phosphate Buffer	$(-9.5\pm2.4) \times 10^{-4}$	0.06710±0.00081	0.69	< 0.05
		Seawater	$(-9\pm18) \times 10^{-5}$	0.05091±0.00077	0.02	0.6